Macromolecules

Article

pubs.acs.org/Macromolecules

PFPE-Based Polymeric ^{19}F MRI Agents: A New Class of Contrast Agents with Outstanding Sensitivity

Cheng Zhang,[†,‡] Shehzahdi Shebbrin Moonshi,[†,‡] Yanxiao Han,[∥] Simon Puttick,[†,‡] Hui Peng,[†,‡] Bryan John Abel Magoling,[†] James C. Reid,[†] Stefano Bernardi,[†] Debra J. Searles,[†,§] Petr Král,[∥,⊥,#] and Andrew K. Whittaker*[,†,‡]

[†]Australian Institute for Bioengineering and Nanotechnology, The University of Queensland, Brisbane, Qld 4072, Australia

[‡]ARC Centre of Excellence in Convergent Bio-Nano Science and Technology, The University of Queensland, Brisbane, Qld 4072, Australia

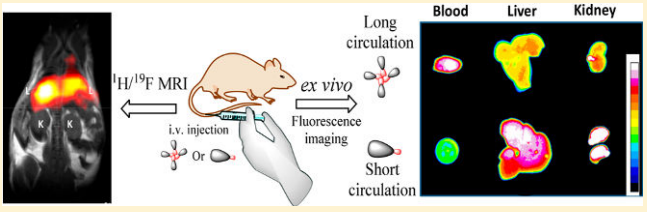
[§]School of Chemistry and Molecular Biosciences, The University of Queensland, Brisbane, Qld 4072, Australia

[∥]Department of Chemistry and [⊥]Department of Physics, University of Illinois at Chicago, Chicago, Illinois 60607, United States

[#]Department of Biopharmaceutical Sciences, University of Illinois at Chicago, Chicago, Illinois 60612, United States

Supporting Information

ABSTRACT: ^{19}F magnetic resonance imaging (MRI) is a powerful noninvasive imaging technique with demonstrated potential for the detection of important diseases. The major challenge in the design of ^{19}F MRI agents is signal attenuation caused by the reduced solubility and segmental mobility of probes with high numbers of fluorine atoms. Careful choice of the fluorinated moiety is required to maintain image quality at the fluorine contents required for high imaging sensitivity. Here we report the synthesis of perfluoropolyether (PFPE) end-functionalized homopolymers of oligo(ethylene glycol) methyl ether acrylate (poly(OEGA)$_m$-PFPE) as highly sensitive ^{19}F MRI contrast agents (CAs). The structural characteristics, conformation and aggregation behavior, ^{19}F NMR relaxation properties, and ^{19}F MR imaging were studied in detail. Dynamic light scattering and molecular dynamics (MD) simulations were conducted and demonstrated that poly(OEGA)$_m$-PFPE with the longest poly(OEGA)$_m$ segments (m = 20) undergoes single-chain folding in water while poly(OEGA)$_{10}$-PFPE and poly(OEGA)$_4$-PFPE with shorter OEGA segments experience multiple-chain aggregation. Long ^{19}F T_2 relaxation times were measured for all poly(OEGA)$_m$-PFPE polymers in PBS and in the presence of serum (>80 ms), and no obvious decrease in ^{19}F T_2 was observed with increasing fluorine content up to ∼30 wt %. Moreover, the signal-to-noise ratio increased linearly with increasing concentration of fluorine, indicating that the PFPE-based polymers can be applied as quantitative tracers. Furthermore, we investigated the *in vivo* behavior, in particular their biodistribution, of the polymers with different aggregation properties. Control over the balance of hydrophobicity and hydrophilicity allows manipulation of the aggregation state, and this leads to different circulation behavior in a murine model. This first report of the synthesis of polymeric PFPE-based ^{19}F MRI CAs demonstrates that these polymers are an exciting new class of ^{19}F MRI CAs with extremely high fluorine content and outstanding imaging sensitivity.



INTRODUCTION

The need to develop highly efficient MRI contrast agents (CAs) for the detection of important disease states at early stages is rapidly becoming a medical diagnostic imperative. Two main classes of CAs have been reported in the literature, namely ^{1}H relaxation agents and ^{19}F imaging agents.[1,2] ^{1}H MRI CAs operate by changing the relaxation properties of ^{1}H spins of the surrounding water molecules and thus highlight pathological features in the diseased tissues by enhancing image contrast. However, the high background signal from water and intrinsic sources of contrast in tissue often make difficult the discrimination of diseased tissue from healthy.[3]

The application of ^{19}F MRI is a promising strategy to overcome these limitations, since the ^{19}F MR signal arises only from the fluorine atoms contained within the fluorinated imaging agents. To achieve comparable image quality as ^{1}H MRI, ^{19}F MRI requires a high concentration of ^{19}F nuclei in the targeted tissue area. For this reason, CAs with a high content of detectable ^{19}F nuclei and a strong tendency to accumulate in the target tissues are required for ^{19}F MRI. During the past few decades, extensive effort has been devoted to the development of partly fluorinated polymers (PFPs) as ^{19}F MRI contrast agents.[4−19] A range of PFPs, including linear polymers, hyperbranched polymers, and dendritic polymers, have been designed and studied as candidate ^{19}F MRI contrast agents. In a typical study from our group,[13] we reported the synthesis of

Received: June 16, 2017
Revised: July 13, 2017
Published: July 25, 2017

ACS Publications © 2017 American Chemical Society

DOI: 10.1021/acs.macromol.7b01285
Macromolecules 2017, 50, 5953−5963

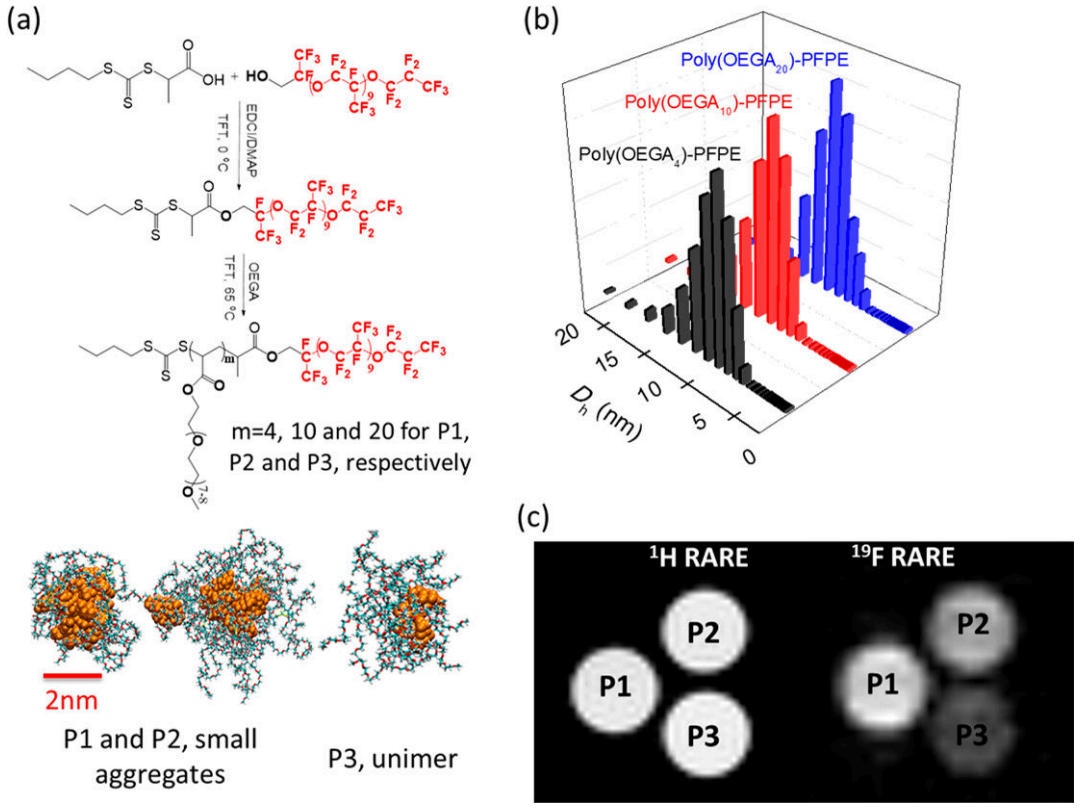


Figure 1. (a) Synthetic scheme and self-assembly behavior of the highly fluorinated PFPE-based ^{19}F MRI CAs with 4 (**P1**), 10 (**P2**), and 20 (**P3**) OEGA units. The scale bar applies to all three snapshots. (b) Number-average size distributions of the three polymers determined by DLS in water. (c) *In vitro* MR spin-echo images of the polymers in PBS at 20 mg/mL. Left and right: ^{1}H and ^{19}F MRI images.

hyperbranched polymers (HBPs) using 2,2,2-trifluoroethyl acrylate (TFEA) as the source of fluorine MR signal, ethylene glycol dimethyl acrylate (EGDMA) as branching monomer, and oligo(ethylene glycol) methyl ether methacrylate (OEGMA) as a hydrophilic monomer to impart water solubility. The polymers incorporated 19 mol % of TFEA, which corresponds to ∼2.5 wt % of fluorine. The ^{19}F NMR relaxation times were measured at 16.4 T, and the longitudinal and transverse relaxation times (T_1 and T_2) were 420 and 54 ms, respectively. Folic acid was conjugated to the hyperbranched copolymer for targeting purposes, and *in vitro* and *in vivo* tests were conducted. The molecules showed high affinity to B16 melanoma cells, and the combination of different imaging modalities within a polymeric nanoparticle provided information on the tumor mass across various size scales *in vivo*, from millimeters down to tens of micrometers. In addition, within our group a wide range of biologically responsive PFPs, such as thermo-, ion-, pH-, and enzyme-responsive polymers, have been developed for tumor-selective ^{19}F MRI imaging by incorporating other functional monomers.[12,14,15,17,20−25] However, a major limitation of these agents preventing their widespread use *in vivo* is the limited sensitivity which is directly related to their modest contents of fluorine atoms.

The low fluorine content (normally below 5 wt %) of the present range of PFPs is a consequence of the limited choice of fluorinated monomers with suitable properties for ^{19}F MRI. TFEA and 2,2,2-trifluoroethyl methacrylate (TFEMA) are the most commonly exploited fluorinated monomers for synthesis of ^{19}F MRI CAs. Previous studies have made clear that novel fluorinated monomers need to be developed for the synthesis of PFPs with higher fluorine content. Perfluoropolyethers (PFPEs), linear perfluorinated polymers, were introduced by Ahrens et al. as suitable components of ^{19}F MRI contrast agents.[26] The linear PFPEs have a simple ^{19}F NMR spectrum arising from >40 equiv fluorine atoms within the CF_2CF_2O monomer repeats and possess a functional group to allow for facile chemical modification.[27−30] The incorporation of a PFPE moiety into a polymer chain will likely produce a material with a significantly higher fluorine content than TFEA or TFEMA. However, to the best of our knowledge, the chemical preparation of water-soluble PFPE-based polymers as ^{19}F MRI contrast agents has not been reported. We demonstrate here that this is an attractive direction in the field of ^{19}F MRI.

Current studies in the field of ^{19}F MRI have been mainly focused on the design of new multifunctional and highly sensitive contrast agents; however, a clear molecular-level understanding of the solution behavior of the fluorinated materials, and how this in turn affects the *in vivo* performance, is not well established. Such an understanding of the fundamental relationships between structure, conformation, and the corresponding ^{19}F MRI performance is critical for the establishment of suitable design criteria for highly sensitive ^{19}F MRI CAs. Previously, the solution properties of partly fluorinated imaging agents have been examined through measurements of molecular size or aggregation state, most usually by dynamic light scattering (DLS), transmission electron microscopy (TEM), ^{19}F NMR spectroscopy, and measurement of NMR relaxation times.[4,11,31] For example, recently Preslar et al.[31] reported the preparation of supramolecular nanostructures formed from fluorinated peptide amphiphiles as "on/off" responsive ^{19}F MRI CAs. They found that the molecules formed aggregates in water which transition

DOI: 10.1021/acs.macromol.7b01285
Macromolecules 2017, 50, 5953−5963

Table 1. Detailed Structural Characteristics, ^{19}F NMR, and MRI Properties of the Poly(OEGA)$_m$-PFPE Polymers

	conv (%)	fluorine content[a] (wt %)	$M_{n,GPC}$[b] (g/mol)	$M_{n,NMR}$[c] (g/mol)	$Đ_M$[b]	D_h[d] (nm)	^{19}F NMR T_1/T_2 (ms)	image SNR[f]
poly(OEGA)$_4$-PFPE	88	28.5	3180	3900	1.06	8.1 ± 0.3	394.6/86.3[e] 397.6/80.6[f]	27.9 ± 0.2
poly(OEGA)$_{10}$-PFPE	89.4	17.0	3410	6600	1.20	9.3 ± 0.1	399.4/93.8[e] 397.1/94.9[f]	20.0 ± 0.2
poly(OEGA)$_{20}$-PFPE	97.2	9.8	6580	11400	1.19	8.3 ± 0.4	404.7/97.4[e] 408.4/100.6[f]	10.1 ± 0.2

[a]The weight percentage of fluorine in the samples. [b]$M_{n,GPC}$ and $Đ_M$ were acquired by SEC in THF using a RI detector (Figure S4). [c]The $M_{n,NMR}$ for the polymers was calculated by considering the integrals of the peaks due to protons H6 (2H), H9 (2H), and the RAFT agent protons H1 (3H) as shown in Figures S5 and S6. [d]D_h was obtained by DLS in PBS, and these are number-average values. The concentration was 20 mg/mL. [e]The ^{19}F NMR T_1/T_2 were measured in PBS/D_2O (90/10, v/v) at 310 K at 9.4 T. [f]The ^{19}F NMR T_1/T_2 were measured in the presence of fetal bovine serum (10% D_2O and 10% FBS in PBS solution) at 310 K at 9.4 T. [g]The experimental image SNR was calculated from the ^{19}F MRI images. The ^{19}F NMR relaxation times and MR image SNR of the poly(OEGA)$_m$-PFPE polymers were acquired for the peak F1.

from cylindrical (on state) to ribbon-like shape (off state) as the pH was increased from 4.5 to 8.0, as confirmed by TEM and ^{19}F NMR spectroscopy. Such observation of the dependence of ^{19}F MRI signal intensity and NMR relaxation times on aggregation state is in line with previous observations by Peng et al. on linear partly fluorinated block copolymers.[11]

Investigations of the behavior of macromolecules at the molecular scale require a combination of experimental and computational techniques (molecular dynamics (MD) simulations) and provide a unique and informative insight into the complex changes experienced by fluorinated polymers in solution. We previously reported the use of a wide range of experimental techniques supported by MD simulations to investigate the changes in conformation experienced by different segments of poly(OEGMA-*co*-TFEA) and second-generation PG2(A) dendronized polymers. The insights obtained into the changes in conformation and association properties demonstrated the power of combining such approaches for understanding properties of complex polymers in solution.[17,20,32]

Here we report, for the first time, the synthesis of novel ^{19}F MRI contrast agents with high fluorine content using a PFPE as a fluorinated, hydrophobic segment, and oligo(ethylene glycol) methyl ether acrylate (OEGA) as the hydrophilic monomer through reversible addition−fragmentation chain-transfer (RAFT) polymerization (Figure 1). The solution behavior (aggregation and/or single-chain folding) of the PFPE-based ^{19}F MRI CAs with different ratios of hydrophobic and hydrophilic segments was studied by a combination of experimental and computational studies. The CAs were conjugated with the fluorescent dye Cy5.5, creating a dual-mode optical-MR imaging contrast agent. The *in vivo* and *ex vivo* studies indicated that the PFPE-based polymers as ^{19}F MRI CAs have exceptional imaging sensitivity and that the hydrophobic−hydrophilic balance plays an important role in determining the *in vivo* behavior. Our results suggest that the PFPEs are promising candidates for the preparation of highly sensitive partially fluorinated polymers as ^{19}F MRI CAs and demonstrate the importance of understanding the effect of hydrophobic−hydrophilic balance on the design of ^{19}F MRI CAs.

EXPERIMENTAL SECTION

Materials. All chemicals were purchased from Sigma-Aldrich unless otherwise stated. Oligo(ethylene glycol) methyl ether acrylate (OEGA, M_w = 480 g/mol), oligo(ethylene glycol) methyl ether methacrylate (OEGMA, M_w = 475 g/mol), and 2,2,2-trifluoroethyl acrylate (TFEA) were passed through basic alumina columns to remove inhibitors prior to use. Monohydroxy perfluoropolyether (PFPE-OH, ∼1450 g/mol) was supplied by Apollo Scientific Ltd., UK. 2,2′-Azobis(2-methylpropionitrile) (AIBN) was recrystallized twice from methanol before use. The RAFT agent 2-(butylthiocarbonothioylthio)propionic acid (PABTC) and 4-cyanopentanoic acid dithiobenzoate (CPADB) were synthesized according to a previously reported procedure.[33] Cyanine5.5 maleimide was purchased from Lumiprobe. Milli-Q water with a resistivity of 18.4 MΩ·cm was used for the relevant experiments. The dialysis tubing with molecular weight cutoff (MWCO) of 2.0 or 3.5 kDa was purchased from Thermo Fisher Scientific Inc. and Spectrum Laboratories Inc., respectively.

Dulbecco's modified Eagle medium (DMEM) with high glucose, phosphate-buffered saline (PBS), Tryple Express, fetal bovine serum (FBS), antibiotic−antimycotic (AA), and ActinRed 555 reagent were purchased from ThermoFisher Scientific. Gelatin was obtained from VWR Chemicals. Mounting media with DAPI was purchased from Vector Laboratories. CellTiter 96 AQ_{ueous} one solution cell proliferation assay (MTS) was purchased from Promega.

Synthesis of PABTC-PFPE Macro-CTA. The PABTC-PFPE macro-CTA was prepared by the EDCI/DMAP catalyzed esterification of carboxylic acid from PABTC RAFT agent with PFPE-OH. A solution of *N*-(3-(dimethylamino)propyl)-*N*′-ethylcarbodiimide hydrochloride (EDCI) (0.288 g, 1.50 mmol) in trifluorotoluene (TFT, 5 mL) was added dropwise to a solution of PFPEs (1.7 g, 1.0 mmol), (propanoic acid)ylbutyl trithiocarbonate (PABTC, 0.381 g, 1.60 mmol), and 4-(dimethylamino)pyridine (DMAP, 0.019 g, 0.16 mmol) in TFT (10 mL) at 0 °C. After complete addition, the reaction mixture was allowed to stir for 20 h at room temperature. The reaction mixture was washed twice with a 1 M sodium hydroxide solution and then twice with distilled water. The organic layer was dried over anhydrous magnesium sulfate, filtered, concentrated under vacuum, and subjected to precipitation into methanol to remove the unreacted PABTC RAFT agent. The desired fraction was concentrated under vacuum to afford the product as a yellow oil for ^{1}H and ^{19}F NMR studies (Figures S1 and S2).

Synthesis of OEGA and PFPE Polymers through RAFT Polymerization. In a typical experiment, PABTC-PFPE macro-RAFT agent (187 mg, 0.11 mmol), OEGA (960 mg, 2.0 mmol), and AIBN (3.28 mg, 0.020 mmol) were dissolved in TFT (2 mL) and sealed in a 10 mL flask fitted with a magnetic stirrer bar. The solution was then deoxygenated by purging thoroughly with nitrogen for 15 min, heated to 65 °C in an oil bath, and allowed to react for 12 h. Upon completing the reaction, the solution was precipitated into hexane and redissolved in THF three times. The precipitate was then dissolved in water and purified by dialysis for 2 days (molecular weight cutoff of 2000 or 3500 Da), yielding a yellow viscous solid after freezer drying. Polymers with a range of compositions were prepared under identical conditions apart from differences in the initial feed amount of OEGA. The detailed structural characteristics of the polymers are summarized in Table 1.

Synthesis of OEGMA and TFEA Polymers through RAFT Polymerization. The typical procedure for preparation of well-defined linear statistical poly(OEGMA-*co*-TFEA) via RAFT polymer-

DOI: 10.1021/acs.macromol.7b01285
Macromolecules 2017, 50, 5953−5963

ization is described as below. OEGMA (1.9 g, 4.0 mmol), TFEA (126 μL, 1.0 mmol), AIBN as initiator (3.28 mg, 0.02 mmol), and CPADB as RAFT agent (27.9 mg, 0.10 mmol) were dissolved in THF (5 mL) to give a [monomer]:[initiator]:[RAFT] ratio of 50:0.2:1. A 25 mL flask with the prepared solution was equipped with a magnetic stirrer bar and sealed with a rubber plug and deoxygenated by purging thoroughly with nitrogen for 15 min before being placed in an oil bath at 65 °C for 12 h. The reaction solution was then placed into an ice bath and exposed to air to terminate the polymerization. The crude mixture was precipitated into hexane, redissolved in THF, reprecipitated into hexane, and then purified by extensive dialysis in water (molecular weight cutoff of 3500 Da) to remove the low molecular species and solvent, finally yielding a pink viscous solid after freeze-drying. Polymers with different TFEA content were prepared under the same condition by simply varying the addition ratio of OEGMA and TFEA. The detailed structural characteristics of the copolymers are summarized in Table S1.

Reduction of the Polymer End Group to Free Thiol. Polymers that contained terminal RAFT agent were reduced to the free thiol by aminolysis in the presence of *n*-hexylamine (4:1) molar ratio to the PFPEs-based polymers and catalytic amount of dimethylphenylphosphine (DMPP) to prevent the formation of a disulfide (1% molar ratio).

Conjugation of Polymer with Cy5.5 Dye. A typical procedure is described here. Into a DMSO solution containing Cy5.5 maleimide (0.185 mg, 0.000 25 mmol), an aqueous solution of P3 (57 mg, 0.0050 mmol) was gradually titrated. The pH was adjusted to ∼7, and the mixture was allowed to react at room temperature in the dark for 12 h. A blue product was obtained after dialysis against water for 2 days and freezer drying. A similar procedure was adopted for conjugation of the dye to **P1** with the same molar ratio of dye to polymer.

Characterization Methods. NMR Spectroscopy. ^{1}H NMR spectra were obtained of solutions of the polymer in $CDCl_3$ using a Bruker Avance 400 MHz (9.4 T) spectrometer to analyze the conversion of monomer to polymer and the structure of the polymers. Solution spectra were measured under the following measurements conditions: 90° pulse width 14 μs, relaxation delay 1 s, acquisition time 4.1, and 32 scans. Chemical shifts are reported relative to the TMS by reference to the residual solvent peak.

^{19}F NMR spectra were acquired using a Bruker Avance 400 MHz spectrometer with either $CDCl_3$ or PBS/D_2O (90/10, v/v) as solvent. The samples tested in the presence of FBS was prepared by addition of 10% FBS in PBS/D_2O (90/10, v/v) solution. Solution spectra were measured under the following measurements conditions: 90° pulse width 15 μs, relaxation delay 1 s, acquisition time 0.73, and 128 scans.

^{19}F spin−spin relaxation times (T_2) were measured using the Carr−Purcell−Meiboom−Gill (CPMG) pulse sequence at 310 K. The samples were dissolved in PBS/D_2O (90/10, v/v) at a concentration of 20 mg/mL. The 90° pulse was determined by dividing with a 360° pulse width, at which the NMR signal is zero. The relaxation delay was 1 s, and the number of scans was 64. The relaxation times for the major peaks only are reported.

^{19}F spin−lattice (T_1) relaxation times were measured using the standard inversion−recovery pulse sequence. For each measurement, the relaxation delay was 2 s and the number of scans was 32. Only values for the major peaks are reported.

Magnetic Resonance Imaging (MRI) of Polymer Solutions. Images of phantoms containing the polymer solutions were acquired on a Bruker BioSpec 94/30 USR 9.4 T small animal MRI scanner. Polymer solutions (20 mg/mL in PBS) were loaded in 5 mm NMR tubes, which were placed in a ^{1}H/^{19}F dual resonator 40 mm volume coil. ^{1}H were acquired for localization of the samples using a rapid acquisition with relaxation enhancement (RARE) sequence (rare factor = 16, TE = 88 ms, TR = 1500 ms, FOV = 40 × 40 mm, matrix = 128 × 128). ^{19}F MRI images were acquired in the same stereotactic space as the ^{1}H image using RARE sequence (rare factor = 32, TE = 11 ms, TR = 1500 ms, number of averages = 128, FOV = 40 × 40 mm, matrix = 64 × 64, measurement time = 25 min 36 s). The ^{19}F MRI signal-to-noise ratio (SNR) is defined as the ratio of the average signal intensity to the standard deviation of the background intensity.

Size Exclusion Chromatography (SEC). Molecular weights and molecular weight distributions were determined by SEC using a Waters Alliance 2690 separations module equipped with a Waters 2414 refractive index (RI) detector, a Waters 2489 UV/vis detector, a Waters 717 Plus autosampler, and a Waters 1515 isocratic HPLC pump. The samples were dissolved in THF at a known concentration (1 mg/mL) and were passed through 0.45 μm filters before testing. The molecular weight was calculated using polystyrene (PS) standards.

Dynamic Light Scattering (DLS). DLS measurements were run on a Nanoseries Zetasizer (Malvern, UK) containing a 2 mW He−Ne laser operating at a wavelength of 633 nm. The polymer concentration was 20 mg/mL, and the scattering angle used was 173°. Each test for the hydrodynamic diameter was repeated three times to provide an average value.

Molecular Dynamics Simulations. Fully atomistic models of poly(OEGA)$_4$-PFPE (**P1**), poly(OEGA)$_{10}$-PFPE (**P2**), and poly-(OEGA)$_{20}$-PFPE polymers (**P3**) were generated, and then the polymers were placed in a simulation cell which was filled with 150 mM NaCl solution to get the fully relaxed structures. To simulate the polymer assembly, five fully relaxed polymer chains were placed into one simulation box in 150 mM NaCl solution. For each of the systems, 20 ns trajectories were collected. All the systems were simulated with NAMD[3] using the CHARMM force field[4−7] in an NPT ensemble at P = 1 bar and T = 300 K, using Langevin dynamics with a damping constant of 0.01 ps^{-1} and a time step of 2 fs. Long-range electrostatic interactions were calculated by PME[8] in the presence of periodic boundary conditions.

MTS Assay. To quantify the potential impact on the cells viability, the 3-(4,5-dimethylthiazol-2-yl)-5-(3-carboxymethoxyphenyl)-2-(4-sulfophenyl)-2*H*-tetrazolium, inner salt (MTS) assay was used. The cells were cultured with the polymers (concentrations from 0 to 15 mg/mL) in a 96-well plate in a final volume of 200 μL with 20K cells per well for 24 h. The MTS solution (20 μL) was added into each well and incubated for 4 h. The plate was briefly shaken on a shaker, and the absorbance of treated and untreated cells was measured using a plate reader at 490 nm.

***In Vivo* Analysis MRI.** Mouse experiments were performed using Female Balb/c nu/nu mice that were bred at the University of Queensland animal house. The mice were 10 weeks old for all experiments. Experiments were repeated three times. Prior to imaging experiments, 50 μL of polymer solution (80 mg/mL in PBS) was injected through the tail vein of the animal (63.3 and 21.8 mg/kg for **P1** and **P3** polymer, respectively). MRI images of live mice were taken on a Bruker BioSpec 94/30 USR 9.4 T small animal MRI scanner. Proton images were acquired using a rapid acquisition with relaxation enhancement (RARE) sequence (rare factor = 16, TE = 15.4 ms, TR = 1500 ms, FOV = 60 × 60 mm, matrix = 256 × 256, measurement time = 1 min 36 s and 8 × 5 mm slices). The ^{19}F images were acquired using RARE sequence (TE = 10 ms, TR = 1500 ms, number of averages = 64, FOV = 60 × 60 mm, matrix = 32 × 32, measurement time = 12 min 48 s, 1 slice or 8 × 2 mm slices). Ethical clearance was obtained from the University of Queensland for live mice testing (AIBN/338/16). The respiration rate of the mouse was monitored at all times during the imaging experiment. The mouse was anaesthetized with an ip injection of 65 mg/kg ketamine, 13 mg/kg xylazine, and 1.5 mg/kg acepromazine.

***Ex Vivo* Fluorescence Imaging.** Following the final time point, the mice treated with polymer were euthanized and the organs excised for *ex vivo* imaging using a Carestream MS FX Pro imaging station (Carestream Health, Inc., Woodbridge, CT). The weight of organs and the volume of blood were recorded for normalization of the fluorescent intensity.

RESULTS AND DISCUSSION

In this work we introduce a series of PFPE-modified RAFT agents for the synthesis of water-soluble ^{19}F MRI contrast agents (CAs) with high imaging sensitivity. As illustrated in Figure 1a, a polymerizable macro-chain-transfer agent was synthesized by standard EDCI/DMAP esterification between

DOI: 10.1021/acs.macromol.7b01285
Macromolecules 2017, 50, 5953−5963

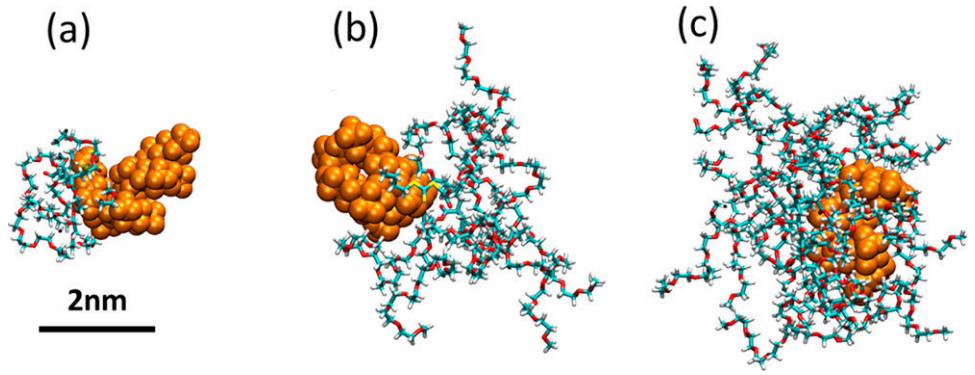


Figure 2. Snapshots of one polymer chain of (a) **P1**, (b) **P2**, and (c) **P3** PFPE-based polymers taken at the end of 20 ns of MD simulation in 150 mM NaCl solution. PFPE segments are shown in orange, and the hydrophilic OEGA parts are in atomistic details. The water molecules have been omitted from the figure, and the relative size of the fluorine atoms was increased for clarity.

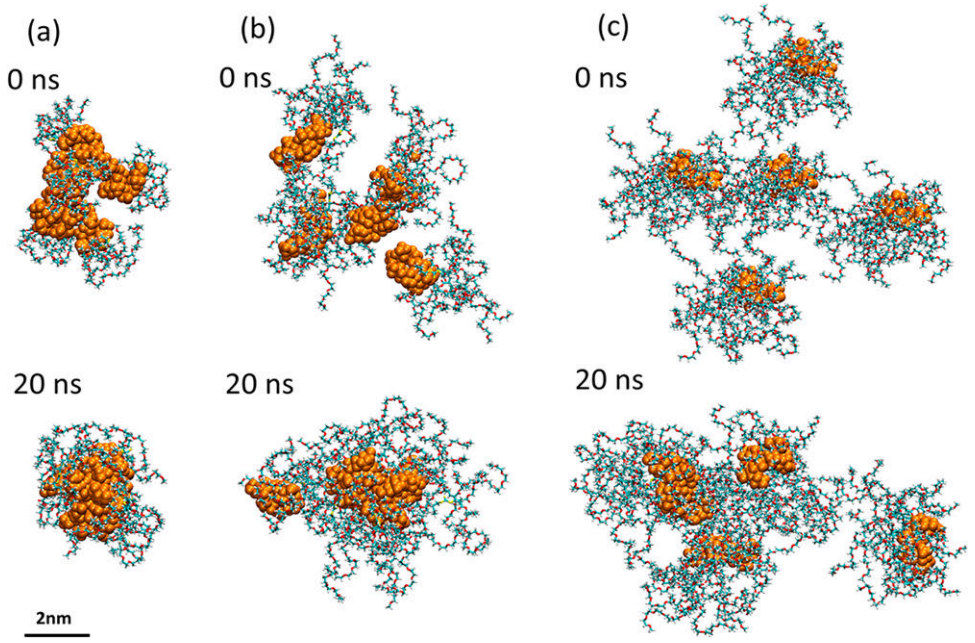


Figure 3. Snapshots of the self-assembly behavior of five polymer chains in 150 mM NaCl solution taken at 0 and 20 ns. (a) **P1**, (b) **P2**, and (c) **P3**. PFPE segments are shown in orange, and the hydrophilic OEGA parts are in atomistic details.

(propionic acid)yl butyl trithiocarbonate (PABTC) and monohydroxy PFPE of molecular weight ~1450 g/mol (PABTC-PFPE macro-CTA). Typical ^{1}H NMR spectra of the PABTC and PABTC-PFPE macro-CTA in $CDCl_3$ and the assignments to the spectra are shown in Figure S1. All peaks in the ^{1}H NMR spectra could be assigned. Moreover, the peak showing extensive splitting located at ~4.6 ppm in the NMR spectrum of the macro-CTA can be assigned to the methylene protons of PFPE segments, indicating the successful synthesis of the macro-CTA. The ^{19}F NMR spectrum of the macro-CTA was also recorded and the peaks assigned successfully as shown in Figure S2. The most intense resonance located at ~−80 ppm in this spectrum is assigned to the fluorinated methyl and methylene groups within the repeat units of the PFPE moiety.

Homopolymers of oligo(ethylene glycol) methyl ether acrylate (poly(OEGA)$_m$-PFPE) with PFPE terminal units were prepared through RAFT polymerization. The overall fluorine content was controlled by varying the molar ratios of OEGA to PABTC-PFPE macro-RAFT agent (4 to 1, 10 to 1, and 20 to 1, for polymers labeled **P1**, **P2**, and **P3**, respectively). The conversion of OEGA to polymer during the polymerization was determined from the integrated intensities in the ^{1}H NMR spectra of the crude samples (Figure S3). Typical ^{1}H and ^{19}F NMR spectra of the poly(OEGA)$_{10}$-PFPE polymer in $CDCl_3$ after purification and the assignments to the spectra are shown in Figure S5. In the ^{1}H NMR spectrum shown in Figure s5a, the methylene protons (2H, $-CH_2O-$) adjacent to the ester groups of the OEGA and the terminal ether oxygen of PFPE appear at ~4.2 ppm (H6) and ~4.6 ppm (H9), respectively. The peak centered at 4.84 ppm (H4′ in the spectrum) can be assigned to the protons of the OEGA bonded directly to the sulfur atoms of the trithiocarbonate RAFT end group. In addition, the peaks in the fluorine NMR spectrum (Figure S5b) were assigned successfully based on previous reports and the integrated intensities of each peak corresponded to the number of fluorine atoms in the chemical structure (Figure s5c).[29,34] It should be noticed that the most intense peak corresponds to the fluorinated methyl and methylene chemical group (−80 ppm, F1 in the spectrum), which will be important for subsequent ^{19}F MRI studies. The

DOI: 10.1021/acs.macromol.7b01285
Macromolecules 2017, 50, 5953−5963

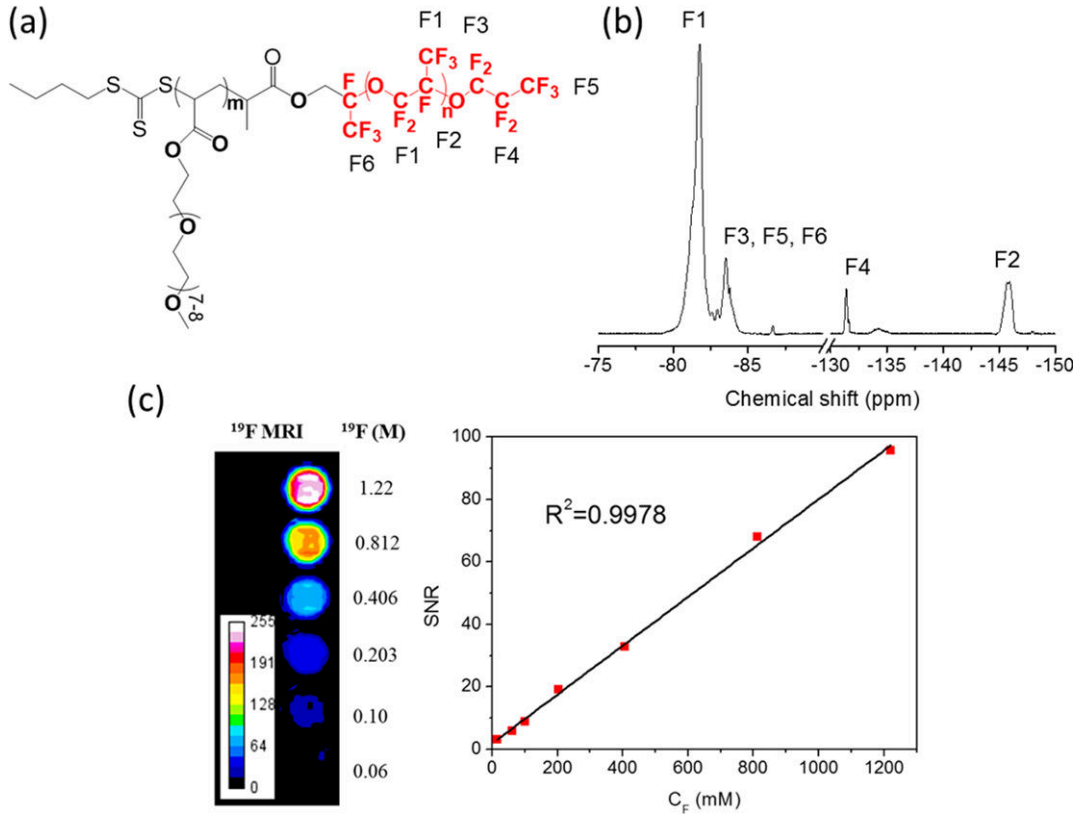


Figure 4. ^{19}F NMR and MRI properties. (a) The chemical structure of the poly(OEGA)$_m$-PFPE polymer. (b) The ^{19}F NMR spectrum of **P1** in PBS/D_2O (v/v 90/10) and assignments to the spectrum. The corresponding spectra of **P2** and **P3** are shown in Figure S7. (c) Left: ^{19}F MRI of **P1** in PBS (400 μL). Right: plot of ^{19}F MRI signal-to-noise ratio as a function concentration of fluorine in solution.

^{1}H and ^{19}F NMR spectra of the poly(OEGA)$_4$-PFPE and poly(OEGA)$_{20}$-PFPE polymers are shown in Figure S6 and indicate the successful synthesis of the poly(OEGA)$_m$-PFPE polymers through RAFT polymerization. All polymers have low molar mass dispersity ($Đ$ < 1.2). The detailed structural characteristics of the polymers are summarized in Table 1.

Previous studies by us have confirmed that for polymeric ^{19}F MRI agents the imaging intensity is dependent on details of molecular association and the extent of segmental motion within the fluorinated segments.[8,11,16] The formation of extensive molecular assembles in solution can result in strong homo- and heteronuclear dipolar interactions and cause severe line broadening and attenuation of the ^{19}F NMR/MRI signal.[8,11,35] As can be observed in Figure 1b and Table 1, the hydrodynamic diameters (D_h) of the PFPE-based polymers in water are all below 10 nm, indicating the molecules in solution are in the form of unimers (**P3**, poly(OEGA)$_{20}$-PFPE) or small aggregates (**P1**, poly(OEGA)$_4$-PFPE, and **P2**, poly(OEGA)$_{10}$-PFPE). To be more explicit, the hydrophobic PFPE segments of the poly(OEGA)$_{20}$-PFPE should be exposed in solution, while poly(OEGA)$_4$-PFPE and poly(OEGA)$_{10}$-PFPE are expected to form a core−shell structure with the PFPE as the core and OEGA comprising the shell (Figure 1a). Large aggregates are not formed with increasing fluorine content, which is important to ensure high mobility of fluorinated segments (and hence long T_2) and obtain sharp and intense ^{19}F NMR signals.

To assist the interpretation of the DLS results, molecular dynamics (MD) simulations were performed on a single polymer chain of the PFPE-based polymers in physiological solution (150 mM NaCl). MD simulations are expected to provide powerful complementary information on the interactions and conformations adopted by the hydrophilic OEGA and hydrophobic PFPE segments. Figure 2 shows the structure of the PFPE-based polymers with different contents of OEGA following ∼20 ns of simulation. Polymers **P1** and **P2** with the shortest OEGA blocks clearly adopt a conformation in which the OEGA and PFPE segments are sharply segregated (Figure 2a,b). In contrast, as shown in Figure 2c, the PFPE segment of **P3** can be wrapped by OEGA chains, indicating that the **P3** can likely exist in solution as a stable unimer.

In order to minimize the exposure of the hydrophobic PFPE segments to water molecules, multiple chains are expected to associate to form small assemblies driven by van der Waals (vdW) and hydrophobic forces. The observed hydrodynamic diameter from DLS of D_h = ∼8−9 nm is consistent with polymers **P1** and **P2** forming such aggregates with OEGA side chains within the shell and the PFPE end group constituting the core as observed in micelle-forming polymeric materials.[36,37] Figure 3a,b which shows the results of MD simulation of five polymer chains of the **P1** and **P2** in water supports this model of aggregation of the smallest two polymers. In the polymer with the highest OEGA content (**P3**), a conformation of single-chain folding rather than multiple-chain aggregation is expected, suggesting that the **P3** polymer can be stabilized by the hydrophilic OEGA segments and that unimers are dominant in solution. Again, the MD simulations support this model of solution behavior (Figure 3c). In polymer **P3**, the steric repulsion and entropic forces of the multiple hydrophilic OEG side chains and the intramolecular hydrophobic interactions within the PFPE segments are able to successfully isolate a signal main chain in solution and prevent

DOI: 10.1021/acs.macromol.7b01285
Macromolecules 2017, 50, 5953−5963

intermolecular aggregation, as confirmed here by DLS measurements.[38] In polymers **P1** and **P2** with lower OEGA content, small intermolecular aggregates are expected to be formed in solution (Figure 3a,b). The combined MD simulation and experimental study of the folding and/or aggregation properties leads to a more complete understanding the solution properties of these PFPE-based polymers.

In order to assess the suitability of the fluorinated polymers as ^{19}F MRI agents, the ^{19}F NMR spectra and relaxation times T_1 and T_2 were measured at a field strength of 9.4 T, and the results shown in Figure 4 and Table 1. The ^{19}F NMR T_1 relaxation times of poly(OEGA)$_m$-PFPE polymers are almost constant for all polymers at approximately 400 ms, indicating similar motional characteristics in the high megahertz frequency regime. The T_2 relaxation times are sensitive to lower frequency motion and the relative displacements of the nuclear spins; both properties depend on the polymer conformation and dynamics. As shown in Table 1, the ^{19}F NMR T_2 of the poly(OEGA)$_m$-PFPE polymers are also approximately independent of fluorine content. These polymers are intended for us as *in vivo* imaging agents; in order to evaluate the effect of the presence of biomolecules in solution on the NMR properties of the PFPE-based polymers, the ^{19}F NMR spectra and relaxation times were also measured for polymers in solutions of fetal bovine serum (FBS). As shown in Figure S8 and Table 1, no obvious peak broadening in the ^{19}F spectrum or change in relaxation times was observed in the presence of serum, indicating the outstanding ^{19}F MRI properties of the PFPE-based polymers can be maintained in a biological environment. Importantly, the poly(OEGA)$_4$-PFPE polymer with the highest fluorine content (28.5 wt %) has a long T_2 at ~86 and 80.6 ms in PBS and in the presence of serum, which should ensure high sensitivity in ^{19}F MRI.

^{19}F MR images of the PFPE-based fluorinated polymers in PBS at a concentration of 20 mg/mL were measured using a spin-echo pulse sequence. The excitation and refocusing pulses were centered on the largest peak in the ^{19}F spectrum at around −80 ppm. The corresponding ^{1}H and ^{19}F MR images of the polymers in PBS are shown in Figure 1c. ^{1}H RARE images are displayed on the left to illustrate the location of the NMR tubes within the resonator. All of the samples could be detected successfully by ^{19}F MRI as shown on the right-hand side of this figure. The most intense images were obtained for poly(OEGA)$_4$-PFPE, which has the highest fluorine content (28.5%), a relatively long ^{19}F NMR T_2 (86.3 ms), and small particle size (<10 nm) in PBS solution. The signal-to-noise ratios (SNRs) calculated from the ^{19}F MRI images are shown in Table 1 and Figure S8c. As can be observed from Figure S8c the SNR of the PFPE-based polymers increases linearly with increasing fluorine content. This is to be expected as the ^{19}F NMR T_1 and T_2 relaxation times are approximately constant for these polymers. The poly(OEGA)$_{20}$-PFPE polymer with the lowest fluorine content (9.8 wt %) has a SNR of ~11, which is sufficient to allow detection of the polymers when administered *in vivo* since the concentration of fluorine in the body capable of being detected by conventional MRI is effectively negligible.[39] The changes in SNR with increasing fluorine content show that the balance between the fluorine content and the mobility/detectability of the fluorine atoms is an important consideration for the design of ^{19}F MRI CAs.

In parallel with this work, the ^{19}F NMR and MRI properties of partly fluorinated copolymers containing 2,2,2-trifluoroacrylate (TFEA, the most commonly used fluorinated monomer in preparation of polymeric ^{19}F MRI CAs) with different fluorine contents were also measured. These are statistical copolymers of OEGMA and TFEA, poly(OEGMA-*co*-TFEA). The structural characteristics, ^{19}F NMR properties, and MR images of those polymers are shown in Tables S1 and S2 as well as Figures S9 and S10. As can be seen in Figure S9c, the SNR of the poly(OEGMA-*co*-TFEA) copolymers initially increases and then decreases with increasing fluorine content in the polymer. The poly(OEGMA$_{14}$-*co*-TFEA$_{13}$) polymer with a moderate fluorine content of 8.3 wt % has the highest SNR of 9 for this series. The decrease in SNR at the higher fluorine contents is caused by the increasingly strong intermolecular association between the hydrophobic units, with an associated decrease in mobility of the fluorinated groups in aqueous solution. The reduced mobility of the fluorinated segments leads to strong dipolar interactions between the nuclear spins and signal decrease in MRI scans. Furthermore, the SNR of the copolymer is always smaller than that of PFPE-based polymers of equivalent fluorine content (Figure S9c), indicating that this PFPE moiety provides superior performance when incorporated in a ^{19}F MRI CA. In previous work from our group, Peng et al. showed that for linear partly fluorinated block copolymers aggregation of the fluorinated segments can lead to strong attenuation of the MRI intensity.[11] Moreover, the ^{19}F MRI signal-to-noise ratios of the PFPE-based polymers and the previous well studied TFEA-based hyperbranched polymers can be calculated use the equation described in eq 1.[40] It can be concluded that the SNR of the PFPE-based polymers (SNR = 24.8, 14.9, and 8.6 for **P1**, **P2**, and **P3**, respectively) is considerably higher than that of the TFEA-based hyperbranched polymers (SNR = 1.6), indicating the PFPE-based polymers have outstanding imaging sensitivity.[10,13]

$$I = N(\mathrm{F})\left[1 - 2\exp\left(\frac{-\left(T_R - \frac{T_E}{2}\right)}{T_1}\right) + \exp\left(\frac{-T_R}{T_1}\right)\right]\exp\left(\frac{-T_E}{T_2}\right) \quad (1)$$

In eq 1, I is the image intensity, N(F) is a measure of the fluorine content in the volume element of the image, T_R and T_E are the pulse sequence repetition and echo times, respectively, and T_1 and T_2 are spin−lattice and spin−spin relaxation times, respectively. The T_R and T_E applied in the current study were 1500 and 10 ms, respectively.

For ^{19}F MRI CAs to provide quantitative imaging information, the SNR must increase linearly with concentration from a few hundred micromolar to several molar.[31] To demonstrate the performance of our CAs, ^{19}F MR images were obtained of phantoms containing solutions of the best candidate polymer, poly(OEGA)$_4$-PFPE, at different concentrations from 1 to 120 mg/mL (15 mM to 1.2 M of fluorine spins). As shown in Figure 3c, samples with higher concentrations of fluorine in solution show brighter ^{19}F MRI images. The plot on the right-hand side of Figure 1c shows that the SNR increases linearly with increasing fluorine concentration in solution, indicating that the SNR was only dependent on the fluorine content and that the T_2 relaxation times must not change significantly over this concentration range. We therefore conclude that the poly(OEGA)$_4$-PFPE polymer is a promising quantitative MR tracer with high sensitivity because the ^{19}F MRI intensity is directly proportional to the local concentration.[5]

DOI: 10.1021/acs.macromol.7b01285
Macromolecules 2017, 50, 5953−5963

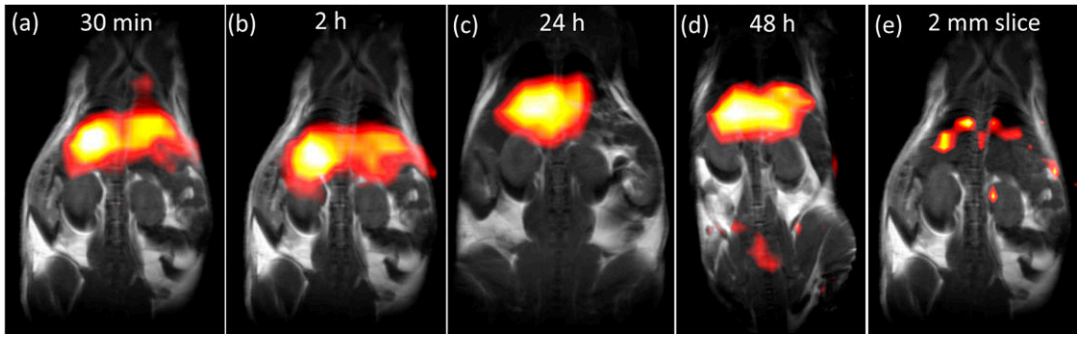


Figure 5. *In vivo* $^{1}H/^{19}F$ MRI at 9.4 T of a mouse following injection with the polymer **P3**. (a–d) MRI images of the mouse 30 min, 2 h, 24 h, and 48 h after tail vein injection. (e) High-resolution ^{19}F MRI with a 2 mm slice thickness 2 h after injection. High-resolution ^{1}H MR images are overlaid with the ^{19}F image.

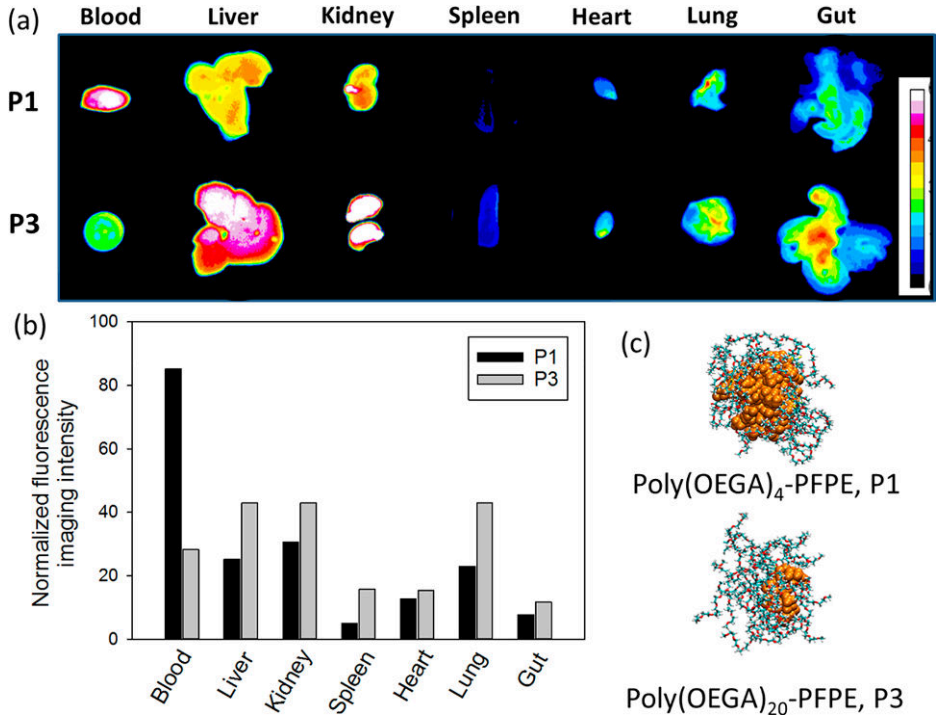


Figure 6. Biodistribution of Cy5.5-labeled **P1** and **P3**. The mice were euthanized 48 h after iv injection of Cy5.5-labeled PFPE-based polymers and the major organs collected for fluorescence imaging. (a) *Ex vivo* fluorescence images of organs. (b) Average fluorescence intensity of each organ normalized to the weight of each organ. (c) Proposed conformation of **P1** and **P3** in solution.

The cytotoxicity of the PFPE-based polymers was tested on MCF-7 cancer cell line via a MTS cell viability assay (Figure S11). The polymers do not display apparent cytotoxicity in the concentration from 2 to 15 mg/mL after incubation for 24 h. In order to demonstrate the potential of the PFPE-based polymers for *in vivo* applications, ^{19}F MRI was performed on a live mouse following the injection of a solution of PFPE-based polymer in PBS via the tail vein. Figure 5 shows the MR images of the mouse of the polymer **P3** at 30 min, 2 h, 24 h, and 48 h after intravenous injection of 50 μL of polymer solution as a concentration of 80 mg/mL in PBS. The high-resolution ^{1}H MR image is overlaid with the ^{19}F MR image. As can be observed in Figure 5a–d, the ^{19}F MRI signals of the polymeric CA can be clearly detected in the mouse using an imaging scan time of ~12 min. In addition, for the first time, high-resolution images with 2 mm slice thickness were obtained to examine the distribution of the contrast agents within specific organs. As shown in Figure 5e, 2 h after injection the image intensity is mainly observed within the region of the liver, kidney, and spleen; accumulation was not detected by ^{19}F MRI in the remaining organs to a significant extent. The accumulation of the PFPE-based polymers in the liver might raise safety concerns for human use; further studies on body clearance and *in vivo* toxicity of these particles will be reported in the near future. Such high-resolution *in vivo* ^{19}F MR images obtained with a short acquisition time confirm that the PFPE-based polymers have sufficient sensitivity for ^{19}F MRI applications. Similar observations were obtained for the **P1** polymers as illustrated in Figure S12. We have therefore demonstrated the first example of PFPE-based polymeric imaging agents being used for ^{19}F MRI and have shown that these agents have outstanding resolution and sensitivity.

It is also worth noting here that CAs **P1** and **P3** appear to be distributed differently within the organs of the mouse (Figure 5 and Figure S12). In order to clarify these observations, a fluorescent dye molecule was conjugated to the PFPE-based

DOI: 10.1021/acs.macromol.7b01285
Macromolecules 2017, 50, 5953–5963

polymer to allow *ex vivo* fluorescent imaging. At 48 h following intravascular injection of the fluorescent polymer **P1**, the mice were sacrificed and the organs excised and imaged using a Carestream MS FX Pro imaging station (Figure 6a). The biodistribution was determined by averaging the fluorescence intensity of each organ normalized to the weight of the organ. As shown in Figure 6b, the **P1** polymer (existing as small aggregates, D_h = 8.1 nm, Figure 6c) was distributed predominantly in the blood, indicating that the **P1** is still circulating after 48 h. The long circulation behavior is due to the PEG chains on the exterior of the small **P1** aggregates which form a hydrophilic and presumably low-fouling corona. This PEG shell reduces the rate of opsonization and prevents rapid uptake by the mononuclear phagocyte system (MPS). This is in agreement with many previous reports that the addition of PEG to the surface of nanoparticles can dramatically reduce uptake by the MPS and increase the circulation time.[41,42] However, in the case of the **P3** polymer (unimer, D_h = 8.3 nm, Figure 6c), greater uptake was evident in the kidneys, liver, and lungs, suggesting a mechanism of increased recognition and clearance. It is likely that exposure of the hydrophobic PFPE segments of the **P3** polymer can dramatically enhance the recognition and filtration by the mononuclear phagocyte system, leading to faster clearance from the body. The results of the DLS measurements and MD simulations which reveal the different aggregation states of **P1** and **P3** are thus supported by the observation of markedly different *in vivo* biodistribution obtained using *ex vivo* fluorescence imaging. Additional experiments are ongoing to understand further these interesting observations. Some data have already shown that the presence of albumin has no effect on the aggregation behavior of the PFPE-based polymers, a result which will be reported separately.

CONCLUSIONS

In summary, we have introduced a versatile PFPE-based platform for the development of highly sensitive molecular imaging agents. These agents have the highest fluorine content reported for polymeric ^{19}F MRI contrast agents. A series of polymers were prepared having different degrees of extension of the PFPE-based RAFT agents with OEGA monomer. The structure, conformation, and aggregation behavior, ^{19}F NMR relaxation properties, and ^{19}F MR imaging were examined in detail. DLS and MD simulations showed that poly(OEGA)$_{20}$-PFPE undergoes single-chain folding in physiological solution while poly(OEGA)$_{10}$-PFPE and poly(OEGA)$_4$-PFPE polymers experience multiple-chain aggregation. A long ^{19}F T_2 was measured for all polymers in a biological environment (>80 ms) with no obvious decrease in ^{19}F T_2 with increasing fluorine content up to as high as 28.5 wt %. The high-resolution *in vivo* ^{19}F MRI with a slice thickness of 2 mm showed clear distribution of the PFPE-based polymers in individual organs. Moreover, the *ex vivo* fluorescence imaging revealed significantly different *in vivo* biodistribution of **P1** and **P3**, which can be explained by differences in aggregation state and extents of presentation of the hydrophobic segments to the solution in these two small polymers. These results are encouraging for future molecular design, in which the PFPE segments can be incorporated within a biocompatible platform with targeting ligands attached for highly sensitive detection of diseases. In summary, the polymeric PFPE-based ^{19}F MRI CAs have high imaging sensitivity and therefore have significant potential for detection of disease at early stages or for tracking of cells and other entities *in vivo*.

ASSOCIATED CONTENT

Supporting Information

The Supporting Information is available free of charge on the ACS Publications website at DOI: 10.1021/acs.macromol.7b01285.

Additional NMR spectroscopy, structure characteristics and MRI phantom images of poly(OEGMA-*co*-TFEA) polymers, and additional *in vivo* MRI images (PDF)

AUTHOR INFORMATION

Corresponding Author

*E-mail: a.whittaker@uq.edu.au (A.K.W.).

ORCID

Simon Puttick: 0000-0003-3909-2646
Debra J. Searles: 0000-0003-1346-8318
Petr Král: 0000-0003-2992-9027
Andrew K. Whittaker: 0000-0002-1948-8355

Notes

The authors declare no competing financial interest.

ACKNOWLEDGMENTS

The authors acknowledge the Australian Research Council (CE140100036, DP0987407, DP110104299, LE0775684, LE0668517, and LE0882357) and the National Health and Medical Research Council (APP1021759) for funding of this research. The Australian National Fabrication Facility, Queensland Node, is also acknowledged for access to some items of equipment. H.P. thanks the University of Queensland for her UQ Postdoctoral Research Fellowship for Women. C.Z. acknowledges the University of Queensland for his Early Career Researcher Grant (UQECR1720289). P.K. acknowledges the NSF Division of Materials Research Grant 1506886. This research was undertaken with support from the Queensland Cyber Infrastructure Foundation (QCIF) and the University of Queensland Research Computing Centre. We acknowledge Dr Nyoman Kurniawan for assistance with the MRI measurements.

REFERENCES

(1) Terreno, E.; Aime, S. MRI Contrast Agents for Pharmacological Research. *Front. Pharmacol.* **2015**, DOI: 10.3389/fphar.2015.00290.

(2) Terreno, E.; Castelli, D. D.; Viale, A.; Aime, S. Challenges for molecular magnetic resonance imaging. *Chem. Rev.* **2010**, *110* (5), 3019−3042.

(3) Pan, D.; Lanza, G. M.; Wickline, S. A.; Caruthers, S. D. Nanomedicine: perspective and promises with ligand-directed molecular imaging. *Eur. J. Radiol.* **2009**, *70* (2), 274−285.

(4) Wang, Z.; Yue, X.; Wang, Y.; Qian, C.; Huang, P.; Lizak, M.; Niu, G.; Wang, F.; Rong, P.; Kiesewetter, D. O.; Ma, Y.; Chen, X. A Symmetrical Fluorous Dendron-Cyanine Dye-Conjugated Bimodal Nanoprobe for Quantitative 19F MRI and NIR Fluorescence Bioimaging. *Adv. Healthcare Mater.* **2014**, *3* (8), 1326−1333.

(5) Yu, W.; Yang, Y.; Bo, S.; Li, Y.; Chen, S.; Yang, Z.; Zheng, X.; Jiang, Z.-X.; Zhou, X. Design and Synthesis of Fluorinated Dendrimers for Sensitive 19F MRI. *J. Org. Chem.* **2015**, *80* (9), 4443−4449.

(6) Du, W.; Nyström, A. M.; Zhang, L.; Powell, K. T.; Li, Y.; Cheng, C.; Wickline, S. A.; Wooley, K. L. Amphiphilic Hyperbranched Fluoropolymers as Nanoscopic 19F Magnetic Resonance Imaging Agent Assemblies. *Biomacromolecules* **2008**, *9* (10), 2826−2833.

(7) Ardana, A.; Whittaker, A. K.; Thurecht, K. J. PEG-Based Hyperbranched Polymer Theranostics: Optimizing Chemistries for Improved Bioconjugation. *Macromolecules* **2014**, *47* (15), 5211−5219.
(8) Peng, H.; Blakey, I.; Dargaville, B.; Rasoul, F.; Rose, S.; Whittaker, A. K. Synthesis and Evaluation of Partly Fluorinated Block Copolymers as MRI Imaging Agents. *Biomacromolecules* **2009**, *10* (2), 374−381.
(9) Nurmi, L.; Peng, H.; Seppala, J.; Haddleton, D. M.; Blakey, I.; Whittaker, A. K. Synthesis and evaluation of partly fluorinated polyelectrolytes as components in 19F MRI-detectable nanoparticles. *Polym. Chem.* **2010**, *1* (7), 1039−1047.
(10) Thurecht, K. J.; Blakey, I.; Peng, H.; Squires, O.; Hsu, S.; Alexander, C.; Whittaker, A. K. Functional Hyperbranched Polymers: Toward Targeted in Vivo 19F Magnetic Resonance Imaging Using Designed Macromolecules. *J. Am. Chem. Soc.* **2010**, *132* (15), 5336−5337.
(11) Peng, H.; Thurecht, K. J.; Blakey, I.; Taran, E.; Whittaker, A. K. Effect of Solvent Quality on the Solution Properties of Assemblies of Partially Fluorinated Amphiphilic Diblock Copolymers. *Macromolecules* **2012**, *45* (21), 8681−8690.
(12) Wang, K.; Peng, H.; Thurecht, K. J.; Puttick, S.; Whittaker, A. K. pH-responsive star polymer nanoparticles: potential 19F MRI contrast agents for tumour-selective imaging. *Polym. Chem.* **2013**, *4* (16), 4480−4489.
(13) Rolfe, B. E.; Blakey, I.; Squires, O.; Peng, H.; Boase, N. R. B.; Alexander, C.; Parsons, P. G.; Boyle, G. M.; Whittaker, A. K.; Thurecht, K. J. Multimodal Polymer Nanoparticles with Combined 19F Magnetic Resonance and Optical Detection for Tunable, Targeted, Multimodal Imaging in Vivo. *J. Am. Chem. Soc.* **2014**, *136* (6), 2413−2419.
(14) Wang, K.; Peng, H.; Thurecht, K. J.; Puttick, S.; Whittaker, A. K. Biodegradable core crosslinked star polymer nanoparticles as 19F MRI contrast agents for selective imaging. *Polym. Chem.* **2014**, *5* (5), 1760−1771.
(15) Zhang, C.; Peng, H.; Whittaker, A. K. NMR investigation of effect of dissolved salts on the thermoresponsive behavior of oligo(ethylene glycol)-methacrylate-based polymers. *J. Polym. Sci., Part A: Polym. Chem.* **2014**, *52* (16), 2375−2385.
(16) Wang, K.; Peng, H.; Thurecht, K. J.; Puttick, S.; Whittaker, A. K. Segmented Highly Branched Copolymers: Rationally Designed Macromolecules for Improved and Tunable 19F MRI. *Biomacromolecules* **2015**, *16* (9), 2827−2839.
(17) Zhang, C.; Peng, H.; Puttick, S.; Reid, J.; Bernardi, S.; Searles, D. J.; Whittaker, A. K. Conformation of Hydrophobically Modified Thermoresponsive Poly(OEGMA-co-TFEA) across the LCST Revealed by NMR and Molecular Dynamics Studies. *Macromolecules* **2015**, *48* (10), 3310−3317.
(18) Wang, K.; Peng, H.; Thurecht, K. J.; Puttick, S.; Whittaker, A. K. Multifunctional hyperbranched polymers for CT/19F MRI bimodal molecular imaging. *Polym. Chem.* **2016**, *7* (5), 1059−1069.
(19) Wang, K.; Peng, H.; Thurecht, K. J.; Whittaker, A. K. Fluorinated POSS-Star Polymers for 19F MRI. *Macromol. Chem. Phys.* **2016**, *217* (20), 2262−2274.
(20) Zhang, C.; Moonshi, S. S.; Peng, H.; Puttick, S.; Reid, J.; Bernardi, S.; Searles, D. J.; Whittaker, A. K. Ion-Responsive 19F MRI Contrast Agents for the Detection of Cancer Cells. *ACS Sensors* **2016**, *1* (6), 757−765.
(21) Takaoka, Y.; Sakamoto, T.; Tsukiji, S.; Narazaki, M.; Matsuda, T.; Tochio, H.; Shirakawa, M.; Hamachi, I. Self-assembling nanoprobes that display off/on 19F nuclear magnetic resonance signals for protein detection and imaging. *Nat. Chem.* **2009**, *1* (7), 557−561.
(22) Yamaguchi, K.; Ueki, R.; Nonaka, H.; Sugihara, F.; Matsuda, T.; Sando, S. Design of Chemical Shift-Switching 19F Magnetic Resonance Imaging Probe for Specific Detection of Human Monoamine Oxidase A. *J. Am. Chem. Soc.* **2011**, *133* (36), 14208−14211.
(23) Takaoka, Y.; Kiminami, K.; Mizusawa, K.; Matsuo, K.; Narazaki, M.; Matsuda, T.; Hamachi, I. Systematic Study of Protein Detection Mechanism of Self-Assembling 19F NMR/MRI Nanoprobes toward Rational Design and Improved Sensitivity. *J. Am. Chem. Soc.* **2011**, *133* (30), 11725−11731.
(24) Fu, C.; Herbst, S.; Zhang, C.; Whittaker, A. K. Polymeric 19F MRI agents responsive to reactive oxygen species. *Polym. Chem.* **2017**, DOI: 10.1039/C7PY00986K.
(25) Zhao, W.; Ta, H. T.; Zhang, C.; Whittaker, A. K. Polymerization-Induced Self-Assembly (PISA) - Control over the Morphology of 19F-Containing Polymeric Nano-objects for Cell Uptake and Tracking. *Biomacromolecules* **2017**, *18* (4), 1145−1156.
(26) Srinivas, M.; Morel, P. A.; Ernst, L. A.; Laidlaw, D. H.; Ahrens, E. T. Fluorine-19 MRI for visualization and quantification of cell migration in a diabetes model. *Magn. Reson. Med.* **2007**, *58* (4), 725−734.
(27) Ahrens, E. T.; Zhong, J. In vivo MRI cell tracking using perfluorocarbon probes and fluorine-19 detection. *NMR Biomed.* **2013**, *26* (7), 860−871.
(28) Ahrens, E. T.; Helfer, B. M.; O'Hanlon, C. F.; Schirda, C. Clinical cell therapy imaging using a perfluorocarbon tracer and fluorine-19 MRI. *Magn. Reson. Med.* **2014**, *72* (6), 1696−1701.
(29) Karis, T. E.; Marchon, B.; Hopper, D. A.; Siemens, R. L. Perfluoropolyether characterization by nuclear magnetic resonance spectroscopy and gel permeation chromatography. *J. Fluorine Chem.* **2002**, *118* (1−2), 81−94.
(30) Srinivas, M.; Turner, M. S.; Janjic, J. M.; Morel, P. A.; Laidlaw, D. H.; Ahrens, E. T. In vivo cytometry of antigen-specific t cells using 19F MRI. *Magn. Reson. Med.* **2009**, *62* (3), 747−753.
(31) Preslar, A. T.; Tantakitti, F.; Park, K.; Zhang, S.; Stupp, S. I.; Meade, T. J. 19F Magnetic Resonance Imaging Signals from Peptide Amphiphile Nanostructures Are Strongly Affected by Their Shape. *ACS Nano* **2016**, *10* (8), 7376−7384.
(32) Zhang, C.; Peng, H.; Li, W.; Liu, L.; Puttick, S.; Reid, J.; Bernardi, S.; Searles, D. J.; Zhang, A.; Whittaker, A. K. Conformation Transitions of Thermoresponsive Dendronized Polymers across the Lower Critical Solution Temperature. *Macromolecules* **2016**, *49* (3), 900−908.
(33) Perrier, S.; Takolpuckdee, P.; Mars, C. A. Reversible addition−fragmentation chain transfer polymerization: end group modification for functionalized polymers and chain transfer agent recovery. *Macromolecules* **2005**, *38* (6), 2033−2036.
(34) Zhang, Z.; Hao, X.; Gurr, P. A.; Blencowe, A.; Hughes, T. C.; Qiao, G. G. Honeycomb Films from Perfluoropolyether-Based Star and Micelle Architectures. *Aust. J. Chem.* **2012**, *65* (8), 1186−1190.
(35) Wang, H.; Raghupathi, K. R.; Zhuang, J.; Thayumanavan, S. Activatable Dendritic 19F Probes for Enzyme Detection. *ACS Macro Lett.* **2015**, *4* (4), 422−425.
(36) Vuković, L.; Khatib, F. A.; Drake, S. P.; Madriaga, A.; Brandenburg, K. S.; Král, P.; Onyuksel, H. Structure and Dynamics of Highly PEG-ylated Sterically Stabilized Micelles in Aqueous Media. *J. Am. Chem. Soc.* **2011**, *133* (34), 13481−13488.
(37) Vuković, L.; Madriaga, A.; Kuzmis, A.; Banerjee, A.; Tang, A.; Tao, K.; Shah, N.; Král, P.; Onyuksel, H. Solubilization of therapeutic agents in micellar nanomedicines. *Langmuir* **2013**, *29* (51), 15747−15754.
(38) Terashima, T.; Sugita, T.; Fukae, K.; Sawamoto, M. Synthesis and Single-Chain Folding of Amphiphilic Random Copolymers in Water. *Macromolecules* **2014**, *47* (2), 589−600.
(39) Pisani, E.; Tsapis, N.; Galaz, B.; Santin, M.; Berti, R.; Taulier, N.; Kurtisovski, E.; Lucidarme, O.; Ourevitch, M.; Doan, B. T.; et al. Perfluorooctyl bromide polymeric capsules as dual contrast agents for ultrasonography and magnetic resonance imaging. *Adv. Funct. Mater.* **2008**, *18* (19), 2963−2971.
(40) Hendrick, R. E.; Kneeland, J. B.; Stark, D. D. Maximizing signal-to-noise and contrast-to-noise ratios in flash imaging. *Magn. Reson. Imaging* **1987**, *5* (2), 117−127.
(41) Jokerst, J. V.; Lobovkina, T.; Zare, R. N.; Gambhir, S. S. Nanoparticle PEGylation for imaging and therapy. *Nanomedicine (London, U. K.)* **2011**, *6* (4), 715−728.
(42) Longmire, M.; Choyke, P. L.; Kobayashi, H. Clearance Properties of Nano-sized Particles and Molecules as Imaging Agents:

DOI: 10.1021/acs.macromol.7b01285
Macromolecules 2017, 50, 5953−5963

Considerations and Caveats. *Nanomedicine (London, U. K.)* **2008**, *3* (5), 703−717.

DOI: 10.1021/acs.macromol.7b01285
Macromolecules 2017, 50, 5953−5963